Journal of Alloys and Compounds 509 (2011) 5173–5176

Contents lists available at ScienceDirect

Journal of Alloys and Compounds

journal homepage: www.elsevier.com/locate/jallcom

High pressure electrical resistivity studies on Ni-doped TiO_2 nanoparticles

K. Karthik*, N. Victor Jaya

Department of Physics, Anna University, Chennai 600 025, India

ARTICLE INFO

Article history:
Received 4 January 2011
Received in revised form 2 February 2011
Accepted 5 February 2011
Available online 1 March 2011

Keywords:
Nanoparticles
Sol–gel
Electrical resistivity
High pressure

ABSTRACT

Electrical resistivity measurement of Ni-doped TiO_2 nanoparticles were performed under high pressure using a Bridgman opposed anvil setup. It is observed that, anatase phase nanoparticles shows a sudden increase in resistivity below the pressure limit of 4 GPa and is attributed to the transition from anatase to rutile phase. In addition, the transition limit is shifted towards lower pressure region with increase in dopant concentration. But, Ni-doped TiO_2 nanoparticles with rutile phase shows a rapid decrease in resistivity up to 5 GPa and thereafter it becomes constant. Samples with constant resistivity behavior are mainly ascribed to the semiconductor-metallic transformation.

1. Introduction

Titanium dioxide (TiO_2) has been extensively studied in recent years because of its potential applications in photocatalysis, dye sensitized solar cells and an anode material for lithium ion batteries [1–5]. Many investigations have been focused on finite size effects and stability of nanocrystalline TiO_2 phases. Size-induced modifications on the physical properties and phase stability of nanocrystalline TiO_2 has played an important role in fundamental studies [6,7]. Numerous studies have reported the detailed investigations of structural behaviors of bulk TiO_2 by Raman spectroscopy and X-ray diffraction. But in this paper, we report a systematic study of the variations of electrical properties as a consequence of structural disorder caused by applying high pressure. High pressure studies leads to the identification of novel material properties such as the perturbed structural and electrical parameters. Microscopic mechanisms and kinetics of solid-state phase transitions for pressure-induced structural transitions in nanocrystalline semiconductors have been investigated using number of studies [8,9]. Electrical resistivity study is an efficient tool to observe the electrical nature of materials properties. However, the resistivity of material much depends on the physical parameters such as pressure, temperature and magnetic field etc., [10,11]. High pressure electrical resistivity measurement is one of the important tool to observe the simultaneous change in phase transformation and electrical transition of metals and semiconductors. The systematic study on nanomaterials under high pressure is important to understand their structural metastabilities and unique properties. The transformation from one phase to another phase must involve specific atomic displacements that change the solid from one symmetry to another accompanied by a change of materials properties.

The objective of the present study is to investigate the pressure induced electrical resistivity behavior of nanoscaled Ni-doped TiO_2 samples for various dopant concentrations. It is of great interest to study the structural metastabilities under high pressure for anatase and rutile phase Ni-doped TiO_2 samples. Although, the results promotes the structural disorder or modified band structure formation under pressure results the variation of electrical resistivity.

2. Experimental

2.1. Preparation of Ni-doped TiO_2

Ni-doped TiO_2 nanoparticles were prepared by sol–gel method using titanium (IV) isopropoxide $[Ti(OCH(CH_3)_2)]_4$ and nickel (II) nitrate hexahydrate as the precursors. In a typical reaction, titanium (IV) isopropoxide (TTIP) and nickel (II) nitrate hexahydrate were dissolved in glacial acetic acid. Deionized water was added to it for hydrolysis and polycondensation reaction. Polyethylene glycol was used as a surfactant. The molar ratio of composition of the Ni-doped TiO_2 (up to 8 mol%) sol was 1:10:200 of $[Ti(OCH(CH_3)_2)]_4$: glacial acetic acid: H_2O. The mixture was stirred for 4 h at room temperature. The resultant homogeneous solution was maintained at 85 °C for gelation process. The gel was then dried and calcined.

2.2. Characterization and measurements

The structures of all samples were identified by X-ray powder diffraction (XRD) at room temperature on a PANalytical X'pert PRO X-ray diffractometer using Cu-Kα radiation (λ = 1.5406 Å) as the X-ray source. The morphology and particle size of the prepared sample was examined by scanning electron microscopy (Hitachi S-3400) and high resolution transmission electron microscopy (HRTEM) on a JEOL JEM 3010 instrument under an acceleration voltage of 300 keV. Raman spectra of all samples were measured with laser Raman spectrometer (Raman R-3000 systems) at room temperature by 532 nm as the laser excitation source.

* Tel.: +91 44 22358689; fax: +91 44 22358700.
E-mail address: karthik_kkdi@yahoo.com (K. Karthik).

0925-8388/$ – see front matter © 2011 Elsevier B.V. All rights reserved.
doi:10.1016/j.jallcom.2011.02.035

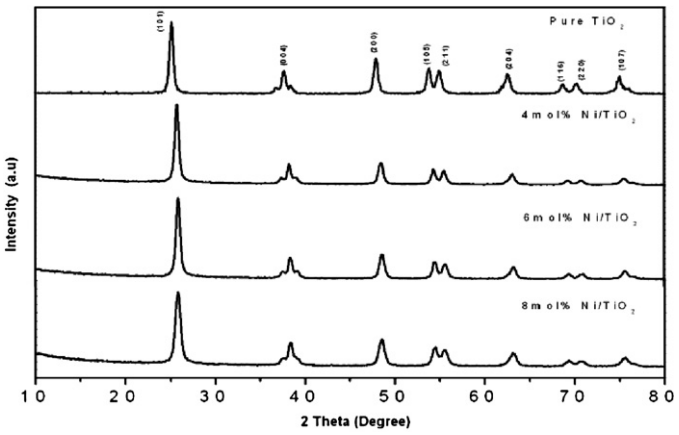

Fig. 1. XRD patterns of pure and Ni-doped TiO_2 calcined at 500 °C.

2.3. High pressure electrical resistivity measurements

The high pressure electrical resistivity studies were carried out using Bridgman opposed anvil setup at room temperature. The anvils are made up of EN24 alloy steel hardened to HRC60. The outer diameter of the anvil is 100 mm and the working face of the anvil is 10 mm diameter. Pyrophyllite is used as a gasket material. The gaskets are 10 mm in outer diameter, 2 mm inner diameter and 0.8 mm thickness. Steatite is used as the pressure transmitting medium. Thin copper wires are used as electrodes to sense the electrical resistivity of the sample. The electrical resistivity of the sample is measured through four probe technique. Pressure is applied to the anvils using a hydraulic press (Lawrence and Mayo 100T).

3. Results and discussions

3.1. Structural and morphological analysis

X-ray powder diffraction pattern of Ni-doped TiO_2 nanoparticles is shown in Fig. 1. It revealed that the diffraction peaks corresponds to the anatase phase tetragonal system of TiO_2 (PCPDF #75-1537). As a consequence, the absence of secondary peaks or related phases should suggest that the doped atoms may incorporate in to the interstitial position or lattice sites of TiO_2. The average particle size is estimated using the Scherrer's relation [12] from the broadening of the major peak. The anatase to rutile phase transformation is accompanied by the high calcination temperature. X-ray powder diffraction pattern of Ni-doped TiO_2 samples calcined at 800 °C is shown in Fig. 2. The diffraction peaks are indexed (using XRDA program) according to the rutile phase tetragonal structure of TiO_2, which is very close to the reported data (PCPDF #88-1175). There is a shift in the peak position to larger angles with the increase in Ni content, reveals the changes in lattice parameter value. Systematically, the increase in lattice parameter value with the increase in particle size is observed, which is due to the lattice expansion of nanocrystals at high calcination temperature [13]. Usually, surface stresses and surface defect dipoles are the two dominant phenomena governing the changes in the lattice parameter value as the particle size is reduced [14,15]. Table 1 shows the lattice constant values and the estimated crystallite sizes of prepared samples.

Table 1
Summary of pure and doped TiO_2.

Sample	Calcination temperature (°C)	Lattice parameters (Å)		Crystallite size (nm)
		a	*c*	
Undoped TiO_2	500	3.797(2)	9.579(3)	18
4 mol% Ni–TiO_2	500	3.751(5)	9.445(7)	17
6 mol% Ni–TiO_2	500	3.744(4)	9.420(2)	16
8 mol% Ni–TiO_2	500	3.734(2)	9.409(6)	14
4 mol% Ni–TiO_2	800	4.521(3)	2.943(2)	67
6 mol% Ni–TiO_2	800	4.537(5)	2.946(8)	71
8 mol% Ni–TiO_2	800	4.547(3)	2.948(3)	76

Anatase phase TiO_2 belongs to the space group D^{19}_{4h} ($I4_1/amd$). According to the factor group analysis, it has six Raman active modes and three infrared active modes [16]. In order to characterize and investigate the presence of any other phase in these compounds, Raman spectra of these samples were recorded and are shown in Fig. 3. The Raman spectrum for anatase single crystal was initially investigated by Ohsaka [17] and totally six allowed modes at around 144 cm^{-1} (E_g), 197 cm^{-1} (E_g), 399 cm^{-1} (B_{1g}), 513 cm^{-1} (A_{1g}), 519 cm^{-1} (B_{1g}) and 639 cm^{-1} (E_g), which are characteristic of first-order Raman active modes [18,19]. Raman spectrum of pure and Ni-doped TiO_2 nanoparticles calcined at 500 °C illustrates the absence of secondary or impurity related phases. Also, the E_g-phonon signal was slightly broadened and shifted to lower frequency region with the increase in Ni-dopant level. This indicates that the incorporation of Ni atom into the TiO_2 host lattice.

Fig. 4(a) shows the scanning electron microscope (SEM) image of 6 mol% Ni-doped TiO_2 nanoparticles calcined at 500 °C. Fig. 4(b) illustrates the transmission electron microscope (TEM) image of the 6 mol% Ni-doped TiO_2 nanoparticles. It is clear that, the particle shows a high monodispersity in size. Fig. 4(c) shows the HRTEM image and reveals a distinct boundary as well as no coalesced part of adjacent TiO_2 particles. In addition, uniform fringes with an interval of 0.34 nm corresponds to the (1 0 1) lattice spacing of anatase phase nanoparticles. This indicates that each nanoparticle consists of a single anatase grain with an average size of 14 nm. The inset of Fig. 4(c) shows the corresponding SAED pattern of 6 mol% Ni-doped

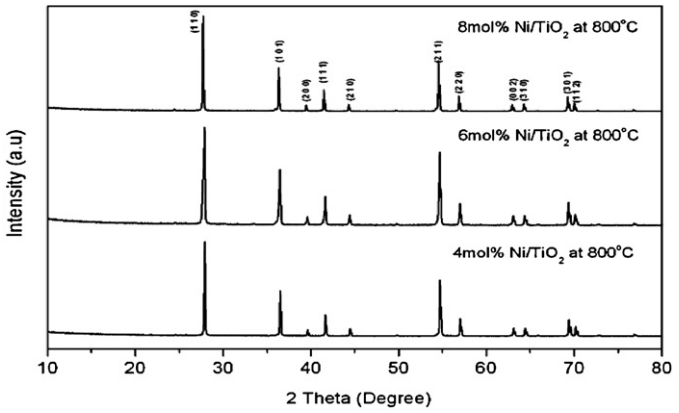

Fig. 2. XRD patterns of Ni-doped TiO_2 calcined at 800 °C.

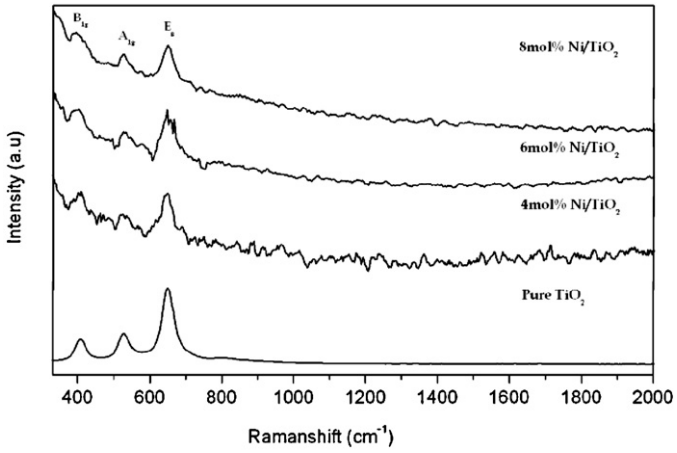

Fig. 3. Raman spectra of pure and Ni-doped anatase TiO_2 nanoparticles.

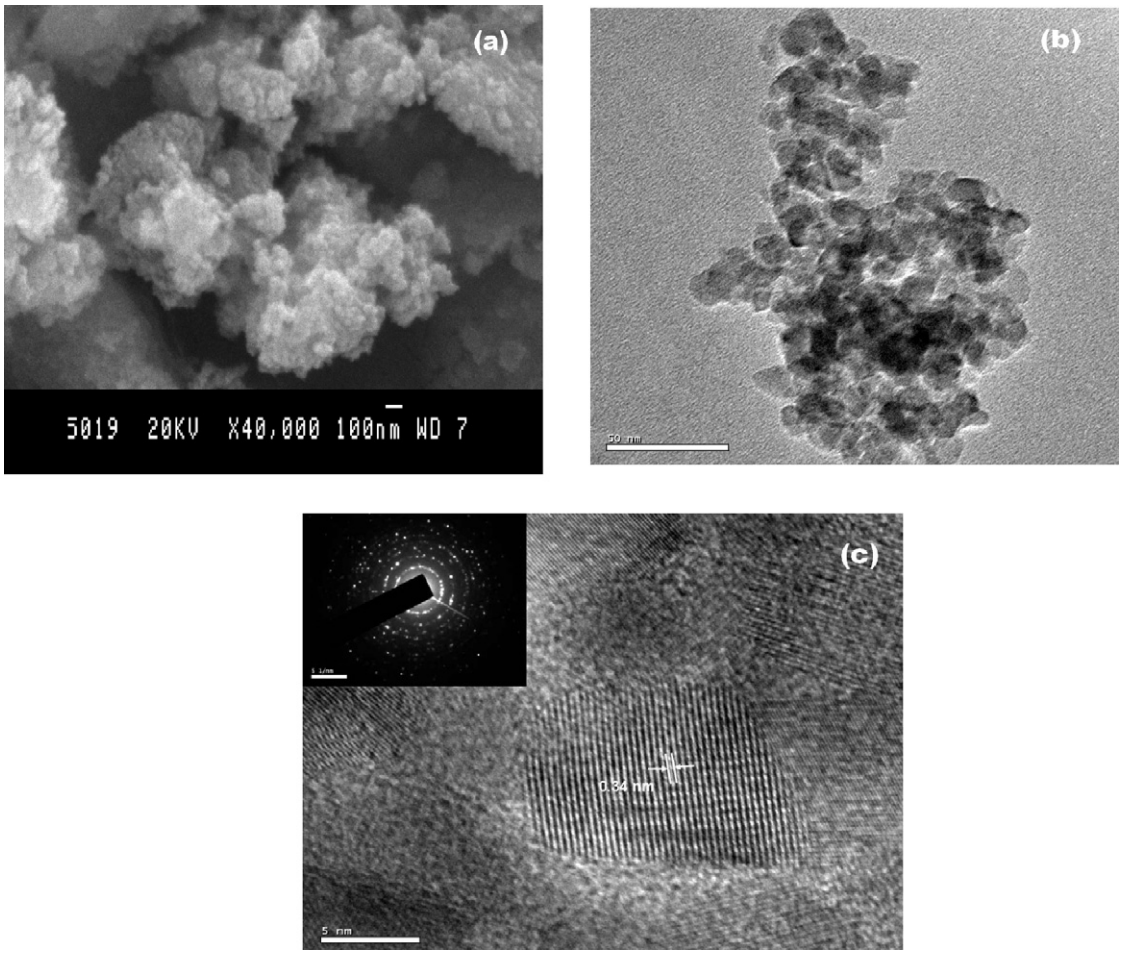

Fig. 4. (a) and (b) show the SEM, TEM images of 6 mol% Ni-doped TiO_2 nanocrystals and (c) denotes the HRTEM image and the inset shows the corresponding SAED pattern respectively.

TiO_2, which indicates that the nanoparticle is highly crystalline in structure, according to the features of diffraction pattern.

3.2. High-pressure electrical resistivity studies

The variation of electrical resistivity under pressure (up to 8 GPa) as a function of Ni concentration is investigated. It is observed that, the electrical resistivity of Ni-doped TiO_2 nanoparticles calcined at 500 °C shows (Fig. 5) an abrupt increase in resistivity value at lower pressure region. This sudden increase in resistivity as a function of Ni concentration is due to the occurrence of structural phase transition from anatase to rutile. The transition pressure is found to shift towards the lower pressure region with the increase in Ni concentration. The resistivity values are found to constant after 4 GPa and it can be due to the transformation of semiconductor-metallic nature of the samples. On the application of high pressure; raises the densities, converting molecular solids to closely packed and thus the resistivity curve is metallic in nature. The high pressure electrical resistivity measurements of Ni-doped TiO_2 nanoparticles calcined at 800 °C is shown in Fig. 6. It is significant that, the electrical resistivity continuously decreased with the increase in pressure. This continuous fall of resistivity is due to the single rutile phase and shows no further evidence of structural transition. Also, the overall resistivity values get decreased with the increase in dopant concentration for both anatase and rutile phase nanoparticles. However, decrease in resistivity is accompanied by the changes in electronic band structure of semiconductor at high pressure, which in turn excites more charge carriers from valence band to conduction band. On the other hand, the concentration of electron and hole greatly depends on impurities and hence the variation of electrical resistivity is mainly attributed to impurity concentration.

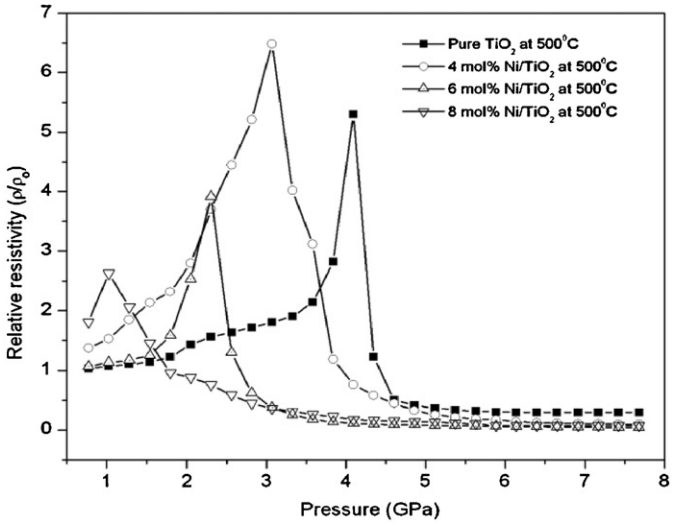

Fig. 5. High pressure electrical resistivity behavior of Ni-doped TiO_2 calcined at 500 °C.

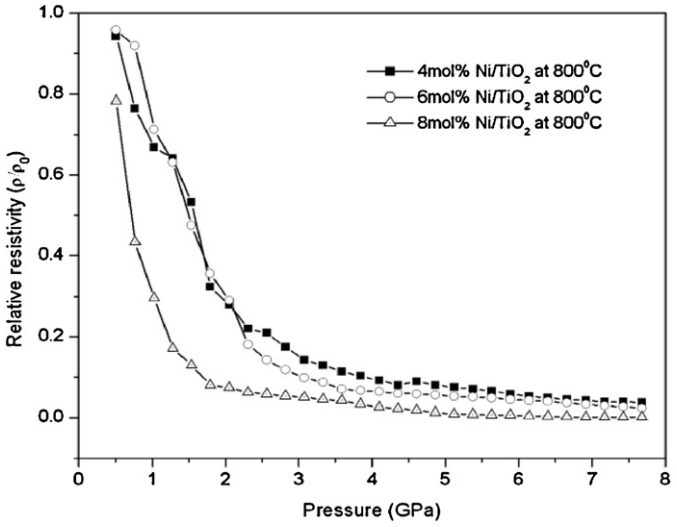

Fig. 6. High pressure electrical resistivity behavior of Ni-doped TiO_2 calcined at 800 °C.

4. Conclusions

In summary, the high pressure electrical resistivity study of Ni-doped TiO_2 nanoparticles as a function of dopant concentration was investigated. The abrupt increase in electrical resistivity of Ni-doped TiO_2 nanoparticles calcined at 500 °C gives hints for possible phase transition which is attributed to structural transition from anatase to rutile with the increase in pressure. It is observed that, the transition pressure decreases with the increase of Ni-concentration. Samples calcined at 800 °C shows the continuous fall of resistivity with the increase in pressure and are constant after 5 GPa. The decrease in resistivity with increase in dopant level indicates that more number of charge carriers is available to conduct current under high pressure.

References

[1] M.R. Hoffmann, S.T. Martin, W. Choi, D.W. Bahnemann, Chem. Rev. 95 (1995) 69.
[2] D.L. Liao, B.Q. Liao, J. Photochem. Photobiol. A: Chem. 187 (2007) 363.
[3] K. Shankar, J. Bandara, M. Paulose, H. Wietasch, O.K. Varghese, G.K. Mor, T.J. LaTempa, M. Thelakkat, C.A. Grimes, Nanoletters 8 (2008) 1654.
[4] D. Kuang, J. Brillet, P. Chen, M. Takata, S. Uchida, H. Miura, K. Sumioka, S.M. Zakeeruddin, M. Gratzel, ACS Nano 2 (2008) 1113.
[5] S.W. Kim, T.H. Han, J. Kim, H. Gwon, H.S. Moon, S.W. Kang, S.O. Kim, K. Kang, ACS Nano 3 (2009) 1085.
[6] H. Zhang, J.F. Banfield, J. Mater. Chem. 8 (1998) 2073.
[7] Z. Zhang, C.C. Wang, R. Zakaria, J.Y. Ying, J. Phys. Chem. B 102 (1998) 10871.
[8] V. Swamy, A. Kuznetsov, L.S. Dubrovinsky, R.A. Caruso, D.G. Shchukin, B.C. Muddle, Phys. Rev. B 71 (2005) 184302.
[9] C. He, C. Gao, Y. Maa, B. Liu, M. Li, X. Huang, A. Hao, C. Yu, D. Zhang, H. Liu, G. Zou, J. Phys. Chem. Sol. 69 (2008) 2227.
[10] R. Selva Vennila, N. Victor Jaya, Mat. Chem. Phys. 89 (2005) 85.
[11] V.E. Arkhipov, V.S. Gaviko, K.M. Demchuk, V.P. Dyakina, A.V. Korolev, Ya.M. MukovskiĬ, É.A. Neifeld, R.V. Pomortsev, JETP Lett. 71 (2000) 114.
[12] B. Cullity, Elements of X-ray Diffraction, Addision-Wesley, Reading, MA, 1987, p. 294.
[13] G. Li, L. Li, J.B. Goates, B.F. Woodfield, J. Am. Chem. Soc. 127 (2005) 8659.
[14] G. Li, J.B. Goates, B.F. Woodfield, L. Li, Appl. Phys. Lett. 85 (2004) 2059.
[15] S. Tsunekawa, K. Ishikawa, Z.Q. Li, Y. Kawazoe, A. Kasuya, Phys. Rev. Lett. 85 (2000) 3440.
[16] T. Bezrodna, G. Puchkovska, V. Shimanovska, J. Baran, Mol. Cryst. Liquid Cryst. 413 (2004) 71.
[17] T. Ohsaka, J. Phys. Soc. Jpn. 48 (1980) 1661.
[18] W. Ma, Z. Lu, M. Zhang, Appl. Phys. A: Mater. Sci. Process. 66 (1998) 621.
[19] M. Popa, L. Diamandescu, F. Vasiliu, C.M. Teodorescu, V. Cosoveanu, M. Baia, M. Feder, L. Baia, V. Danciu, J. Mater. Sci. 44 (2009) 358.